Free Radical Biology & Medicine 50 (2011) 1151–1162

Contents lists available at ScienceDirect

Free Radical Biology & Medicine

journal homepage: www.elsevier.com/locate/freeradbiomed

Original Contribution

A novel synthetic protoapigenone analogue, WYC02-9, induces DNA damage and apoptosis in DU145 prostate cancer cells through generation of reactive oxygen species

Huei-Mei Chen [a,b], Fang-Rong Chang [b,c,d], Ya-Ching Hsieh [a], Yu-Jen Cheng [e], Kun-Chou Hsieh [e], Lih-Min Tsai [a], An-Shen Lin [b], Yang-Chang Wu [b,f,g,*], Shyng-Shiou Yuan [a,h,i,**]

[a] Department of Medical Research, E-DA Hospital, Kaohsiung 824, Taiwan, Republic of China
[b] Graduate Institute of Natural Products, College of Pharmacy, Taiwan, Republic of China
[c] Cancer Center, University Hospital, Kaohsiung Medical University, Kaohsiung 807, Taiwan, Republic of China
[d] Department of Marine Biotechnology and Resources, National Sun Yat-sen University, Kaohsiung 804, Taiwan, Republic of China
[e] Division of Thoracic Surgery, Department of Surgery, E-DA Hospital/I-Shou University, Kaohsiung County, Taiwan, Republic of China
[f] Graduate Institute of Integrated Medicine, College of Chinese Medicine, Taiwan, Republic of China
[g] Natural Medicinal Products Research Center, University Hospital, China Medical University, Taichung 40402, Taiwan, Republic of China
[h] Department of Obstetrics and Gynecology, E-DA Hospital, Kaohsiung 824, Taiwan, Republic of China
[i] Department of Biological Science and Technology, I-Shou University, Kaohsiung 824, Taiwan, Republic of China

ARTICLE INFO

Article history:
Received 19 October 2010
Revised 7 December 2010
Accepted 7 January 2011
Available online 20 January 2011

Keywords:
WYC02-9
ROS
Prostate cancer
γ-H2A.X, $\Delta\Psi_m$ decrease
Free radicals

ABSTRACT

The protoapigenone analogue WYC02-9, a novel synthetic flavonoid, has been shown to act against a variety of experimental tumors. However, its effects on prostate cancer and its mechanism of action are unknown. Thus, WYC02-9 was investigated for its cytotoxicity against DU145 prostate cancer cells, as was the underlying mechanisms by which WYC02-9 might induce DNA damage and apoptotic cell death through reactive oxygen species (ROS). WYC02-9 inhibited the cell growth of three prostate cancer cell lines, especially DU145 cells. In DU145 cells, WYC02-9 increased the generation of intracellular ROS, followed by induction of DNA damage and activation of the ATM–p53–H2A.X pathway and checkpoint-related signals Chk1/Chk2, which led to increased numbers of cells in the S and G2/M phases of the cell cycle. Furthermore, WYC02-9 induced apoptotic cell death through mitochondrial membrane potential decrease and activation of caspase-9, caspase-3, and PARP. The above effects were all prevented by the ROS scavenger *N*-acetylcysteine. Administration of WYC02-9 in a nude mouse DU145 xenograft model further identified the anti-cancer activity of WYC02-9. These findings therefore suggest that WYC02-9-induced DNA damage and mitochondria-dependent cell apoptosis in DU145 cells are mediated via ROS generation.

Flavonoids are well-documented inhibitors of cell growth in various cancer cells [1,2]. Protoapigenone (Fig. 1A), a novel plant-derived natural flavonoid isolated from *Thelypteris torresiana* (Gaud.), has potent cytotoxicity against several human cancer cell lines through oxidative stress-induced cell cycle arrest and apoptosis [3–5]. There are three compounds of flavonoids, including apigenin, kaempferol, and quercetin, with structures similar to that of protoapigenone. However, these three compounds displayed low activity against various human cancer cell lines [3]. The different characteristics of the flavonoid skeleton attracted our interest in performing structure–activity relationship studies. The novel plant-derived natural flavonoid, the synthesized protoapigenone (named WYC02), and its analogue, WYC02-9 (with a C-7 methoxy group), are cytotoxic to various cancer cells, including HepG2, Hep3B, MDA-MB-231, MCF-7, and A549 [3].

WYC02 is one of the quinone compounds with chemotherapeutic effects on human cancers [7–9] through generation of reactive oxygen species [9–11]. Excessive production of ROS has been shown to cause cell death by DNA damage-induced cell cycle arrest in several cancer cells [12–17]. ROS production also causes a decrease in mitochondrial transmembrane potential ($\Delta\Psi_m$) as well as the release of cytochrome *c* and leads to mitochondrial-dependent apoptosis in a variety of human cancer cells [18–20].

Prostate cancer (PCA) is the most frequently diagnosed malignancy in elderly males and the second leading cause of cancer-related deaths in the United States [21,22]. It has also become a major malignancy in

Abbreviations: ROS, reactive oxygen species; NAC, *N*-acetyl-L-cysteine; PCA, prostate cancer; $\Delta\Psi_m$, mitochondrial membrane potential; ATM, ataxia telangiectasia mutated; DCF-DA, 2′,7′-dichlorofluorescin diacetate; XTT, tetrazolium salt; DMSO, dimethyl sulfoxide; PI, propidium iodide; DSB, DNA double-strand break; IC_{50}, the half-maximal inhibitory concentration; BUN, blood urea nitrogen; Cr, creatinine; AST, aspartase; ALT, alanine; PARP, poly(ADP-ribose) polymerase.

* Correspondence to: Y.-C. Wu, Graduate Institute of Natural Products, College of Pharmacy, Taiwan, Republic of China. Fax: +886 4 220 60248.
** Correspondence to: S.-S.F. Yuan, Department of Obstetrics and Gynecology, E-DA Hospital, Kaohsiung 824, Taiwan, Republic of China. Fax: +886 7 6155352.
E-mail addresses: yachwu@mail.cmu.edu.tw (Y.-C. Wu), yuanssf@ms33.hinet.net (S.-S. Yuan).

0891-5849/$ – see front matter © 2011 Elsevier Inc. All rights reserved.
doi:10.1016/j.freeradbiomed.2011.01.015

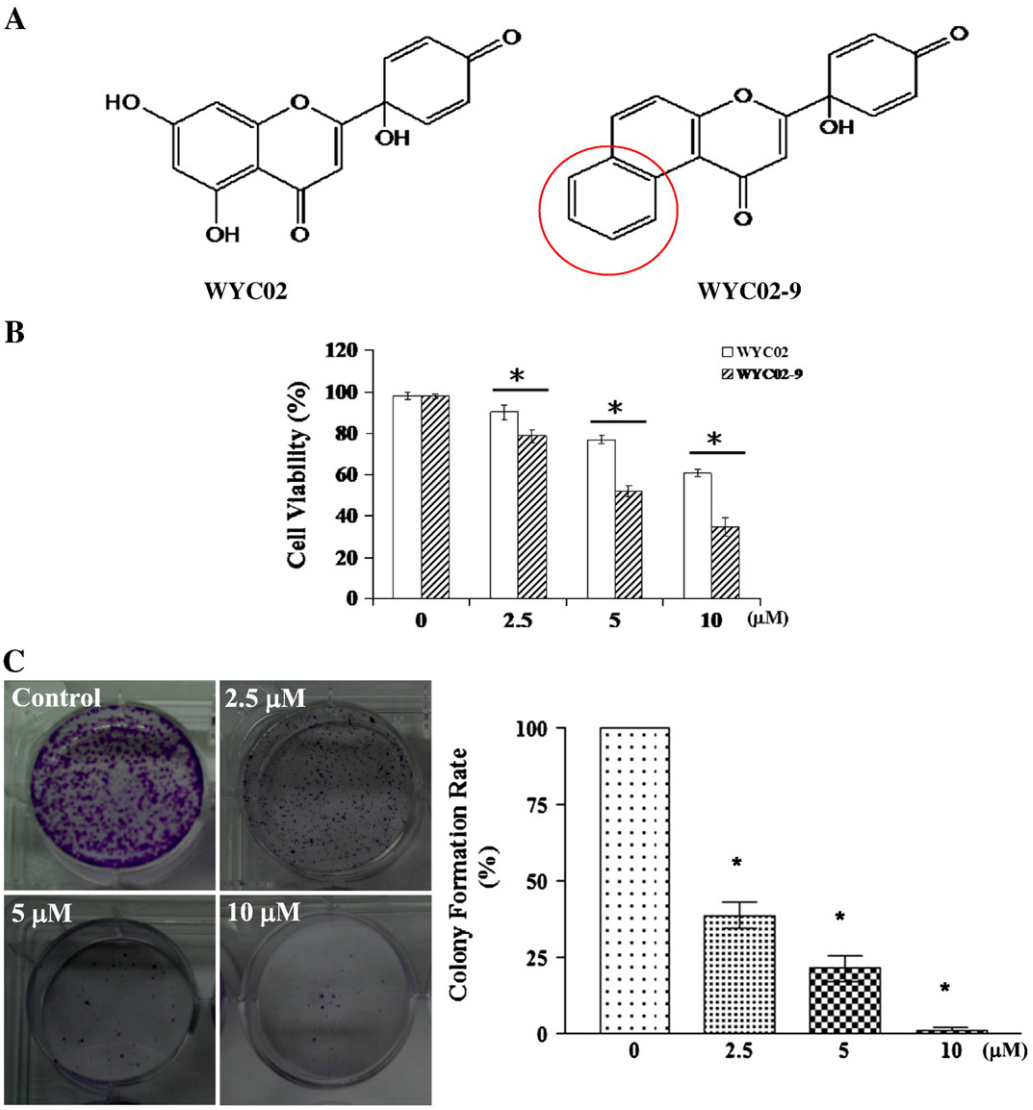

Fig. 1. Effects of WYC02 and WYC02-9 on DU145 cell viability. (A) Chemical structure of WYC02 and its analogue WYC02-9. (B) Effects of WYC02 and its analogue WYC02-9 on DU145 cell viability. DU145 cells were treated with various concentrations of WYC02 or WYC02-9 for 24 h and assessed by viability assay. Data are presented as means ± SD of three independent experiments. *$P<0.05$ compared with the respective controls treated with WYC02-9 alone. (C) Effect of WYC02-9 on DU145 cell colony formation, as evaluated by clonogenic assay. Data are presented as means ± SD of three independent experiments. *$P<0.05$ compared with the untreated control.

many Asian countries in the past 2 decades [23,24]. Although androgen-ablation therapy is one of the mainstays of PCA treatment, PCA often rebounds because of drug resistance [25,26]. Therefore in recent years, natural botanicals have attracted more attention because of their potential role as cancer-chemopreventive agents [24,27,28] and more effort has been put into identifying novel botanicals that selectively target tumor cell growth without affecting normal cells [25,29].

In this study, we explored the potential of the protoapigenone analogue WYC02-9 against PCA using DU145 cancer cells as the model. Herein, we show that WYC02-9 was able to induce DNA damage, increase cells in S and G2/M phases, and increase mitochondrial-dependent apoptotic cell death by generating ROS in DU145 cells. We also show that administration of WYC02-9 inhibited DU145 xenograft growth in nude mice.

Material and methods

Origins of WYC02 and WYC02-9

In our previous study, we isolated the novel flavonoid protoapigenone, from *T. torresiana* (Gaud.), which is cytotoxic to several human cancer cell lines [3–6]. To develop more effective anti-cancer agents based on this novel plant-derived natural flavonoid, the first total synthesis of protoapigenone (renamed WYC02 in this study for synthetic protoapigenone) and its derivatives was accomplished [3]. The chemical structures of WYC02 and WYC02-9 are shown in Fig. 1A.

Drugs and chemicals

DMEM and RPMI 1640 were obtained from Gibco (Invitrogen, Carlsbad, CA, USA). Fetal bovine serum and penicillin/streptomycin/amphotericin B were obtained from Biological Industries (Haemek, Israel). Rhodamine 123 and H_2DCF-DA were obtained from Molecular Probes (Eugene, OR, USA). Tetrazolium salt (XTT) was purchased from Sigma Chemical Co. (St. Louis, MO, USA). Antibodies recognizing γ-H2A.X(Ser139), p-ATM(Ser1981), p-p53, p-Chk1(Ser296), p-Chk2(Ser68), and ATM (ataxia telangiectasia mutated) were purchased from Cell Signaling Technology (Beverly, MA, USA). Chk1, Chk2, and H2A.X were purchased from GeneTex, Inc. (Irvine, CA, USA). Caspase-3 and β-actin were obtained from Abcam (Cambridge, MA, USA). Primary antibodies against poly(ADP-ribose) polymerase (PARP), caspase-9, and p53 were purchased from Santa Cruz Biotechnology (Santa Cruz, CA, USA). DMSO,

N-acetylcysteine (NAC), propidium iodide (PI), and all other chemicals were obtained from Sigma Chemical Co.

Cell cultures

The cancer cell lines DU145, PC-3, and LNCaP were purchased from the ATCC (Manassas, VA, USA). DU145 and PC-3 cells were grown in DMEM and LNCaP cells were grown in RPMI 1640. Both media were supplemented with 10% fetal bovine serum and penicillin/streptomycin/amphotericin B.

XTT cell proliferation assay and colony formation assay

Cells were plated out at a density of 8000 cells/well in 96-well microtiter plates. After 24 h incubation, the cells were treated with WYC02 and WYC02-9 for 48 h and cell proliferation was determined by XTT colorimetric assay (Roche Molecular Biochemicals, Indianapolis, IN, USA). Briefly, the culture medium was removed, and 100 μl of fresh culture medium with 50 μl of preformulated XTT mixed reagent was added. The culture plate was incubated at 37 °C for 4 h. The optical density was measured at 490 nm with reference wavelength at 650 nm by using an ELISA reader. The 50% inhibitory concentration (IC_{50}) was calculated.

To determine long-term effects, cells were treated with WYC02-9 at various concentrations for 3 h. After being rinsed with fresh medium, cells were allowed to grow for 10 days to form colonies, which were then stained with crystal violet (0.4 g/L; Sigma Chemical Co.).

Cell viability assay

Cells were plated out at a density of 80,000 cells/ml in six-well microtiter plates. After treatment with WYC02 or WYC02-9 for 24 h, cell viability was determined using a Countess automated cell counter (Invitrogen). Briefly, the culture medium was removed and then washed with cold 1× PBS and suspended in 500 μl of 1× PBS. Then 10 μl of sample was mixed with 10 μl of trypan blue, and pipetted into a Countess chamber slide for cell counting. Detailed procedure was followed according to the manufacturer's protocol (Invitrogen).

Detection of intracellular ROS accumulation and determination of $\Delta\Psi_m$

The levels of ROS and $\Delta\Psi_m$ were examined by flow cytometry using H_2DCF-DA and rhodamine 123, respectively. The detailed procedure was followed according to a previous report [14]. After treatment with WYC02-9, the cells were loaded with 20 μM H_2DCF-DA and 10 μM rhodamine 123 and incubated at 37 °C for 30 min in the dark. The cells were then collected, washed, and resuspended in PBS and analyzed immediately using flow cytometry. Mean fluorescence intensity detected by the FL1 channel was analyzed using CellQuest software (Becton–Dickinson, San Jose, CA, USA).

Neutral comet assay for detection of DNA double-strand breaks (DSBs)

The assay was carried out using a CometAssay kit (Trevigen, Gaithersburg, MD, USA) following the manufacturer's protocol for the neutral comet assay. Briefly, DU145 cells were treated with WYC02-9 (10 μM) for the indicated time periods, and the treated cells were then

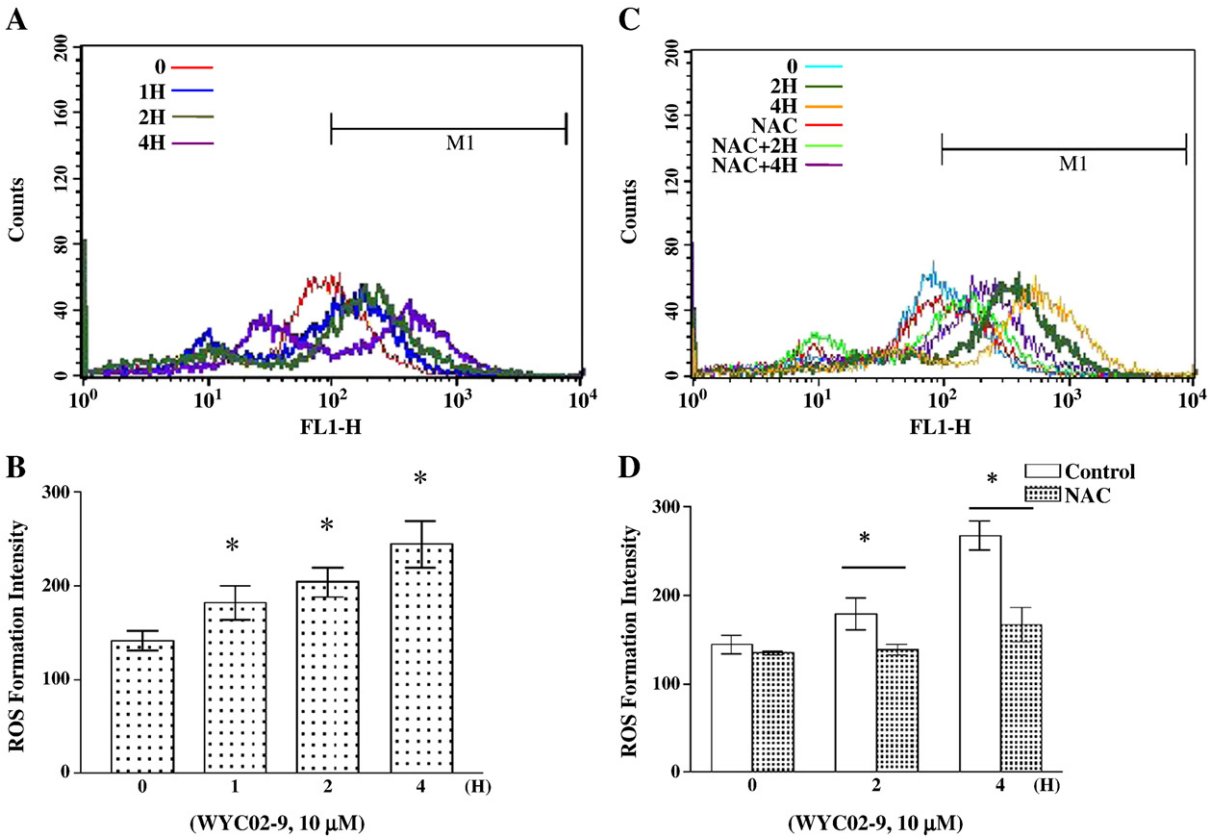

Fig. 2. Effect of WYC02-9 on cellular ROS accumulation in DU145 cells. (A) Effect of WYC02-9 (10 μM) on intracellular ROS formation in DU145 cells. (B) Quantitative analysis of the results of (A) presented as means ± SD of three independent experiments. *P<0.05 compared with the untreated control. (C) Effect of NAC pretreatment on WYC02-9-incduced intracellular ROS formation. (D) Quantitative analysis of the results of (C) presented as means ± SD of three independent experiments. *P<0.05 compared with the respective controls treated with WYC02-9 alone. ROS, reactive oxygen species; NAC, *N*-acetylcysteine.

mixed with 1% low-melting-point agarose at a ratio of 1:10 (v/v). Then 75 µl of the mixture was immediately pipetted onto a CometSlide and allowed to set at 4 °C for 30 min in the dark. The slides were immersed in ice-cold lysis solution (Trevigen) for 30 to 60 min and the slides were then placed in a horizontal electrophoresis apparatus and electrophoresed in 1× TBE (90 mM Tris–HCl, 90 mM boric acid, and 2 mM EDTA, pH 8.0) at 20 V for 10 min. The samples were then fixed in 70% ethanol and dried before being stained with 1:10,000 SYBR Green I (Trevigen) to visualize cellular DNA.

The fluorescence images were analyzed using the TriTek Comet Image program to circumscribe the "head" and the "tail" regions of each comet and the integrated fluorescence value of each defined area was recorded. The comet length, an indicator of the extent of DNA damage, was measured from the trailing edge of the nucleus to the leading edge of the tail.

Immunostaining of γ-H2A.X foci

Cells were seeded at 1×10^4 cells/well in eight-well chamber slides (Lab-Tek II) and incubated for 24 h before treatment. After WYC02-9 treatment alone or pretreatment with NAC followed by WYC02-9, the cells were fixed with 4% paraformaldehyde. The cells were incubated with a 1:200 dilution of antibody γ-H2A.X at 4 °C overnight, followed by goat anti-rabbit secondary antibody conjugated with the fluorochrome FITC (Santa Cruz Biotechnology) for 1 h at room temperature and viewed with a Zeiss AxioCam MRm fluorescence microscope (Germany) with excitation at 494 nm and 520 nm emission filter.

Immunoblotting analysis

Immunoblotting was performed as previously described [14,30]. The chemiluminescent signal was captured by a UVP BioSpectrum 500 imaging system (Level Biotechnology, USA). The abundance of protein was analyzed by quantification of the intensity of the corresponding band.

Measurement of cell cycle/DNA content

Cell cycle distribution was determined by FACS analysis. DU145 cells at a concentration of 2×10^5 were seeded onto six-well microtiter plates and treated with WYC02-9 or combined with NAC for the desired periods of time. The cells were collected and fixed overnight in 70%

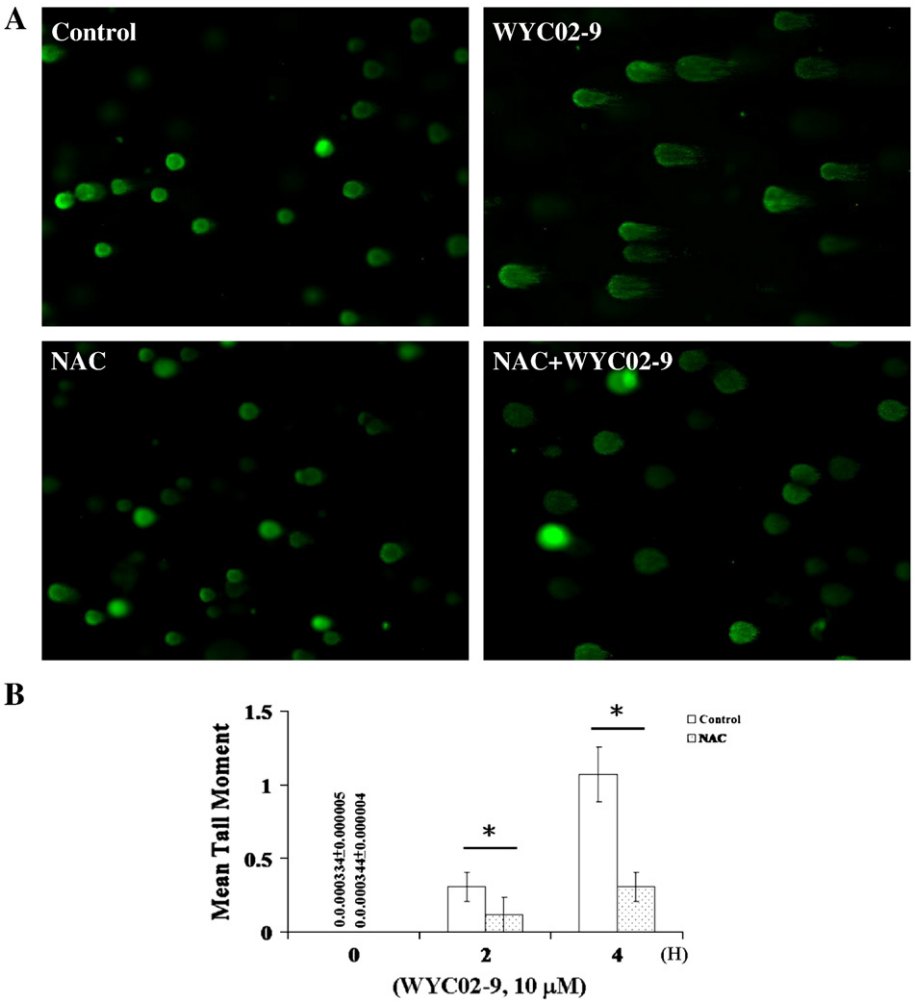

Fig. 3. Effect of WYC02-9 on induction of double-strand breaks in DU145 cells. (A) Representative images of comet tails due to chromosomal DNA double-strand breaks in WYC02-9 (10 µM)-treated DU145 cells compared to the untreated control. (B) Effect of WYC02-9 on comet tail formation. Data are presented as means ± SEM of three independent experiments and a minimum of 50 cells were included in each experiment (for details, please see Material and methods). *P<0.05 compared with the respective controls treated with WYC02-9 alone. (C) Effect of WYC02-9 on induction of γ-H2A.X focus formation in DU145 cells. Cells were fixed and incubated with antibodies against γ-H2A.X, followed by secondary antibodies conjugated with the fluorochrome FITC. Nuclei were stained with DAPI. After immunostaining, cells were viewed by fluorescence microscope (original magnification × 1000). (D) Quantitative analysis of the results of (C) presented as means ± SD of three independent experiments as a minimum of 100 cells were included in the experiment. *P<0.05 compared with untreated control. NAC, *N*-acetylcysteine.

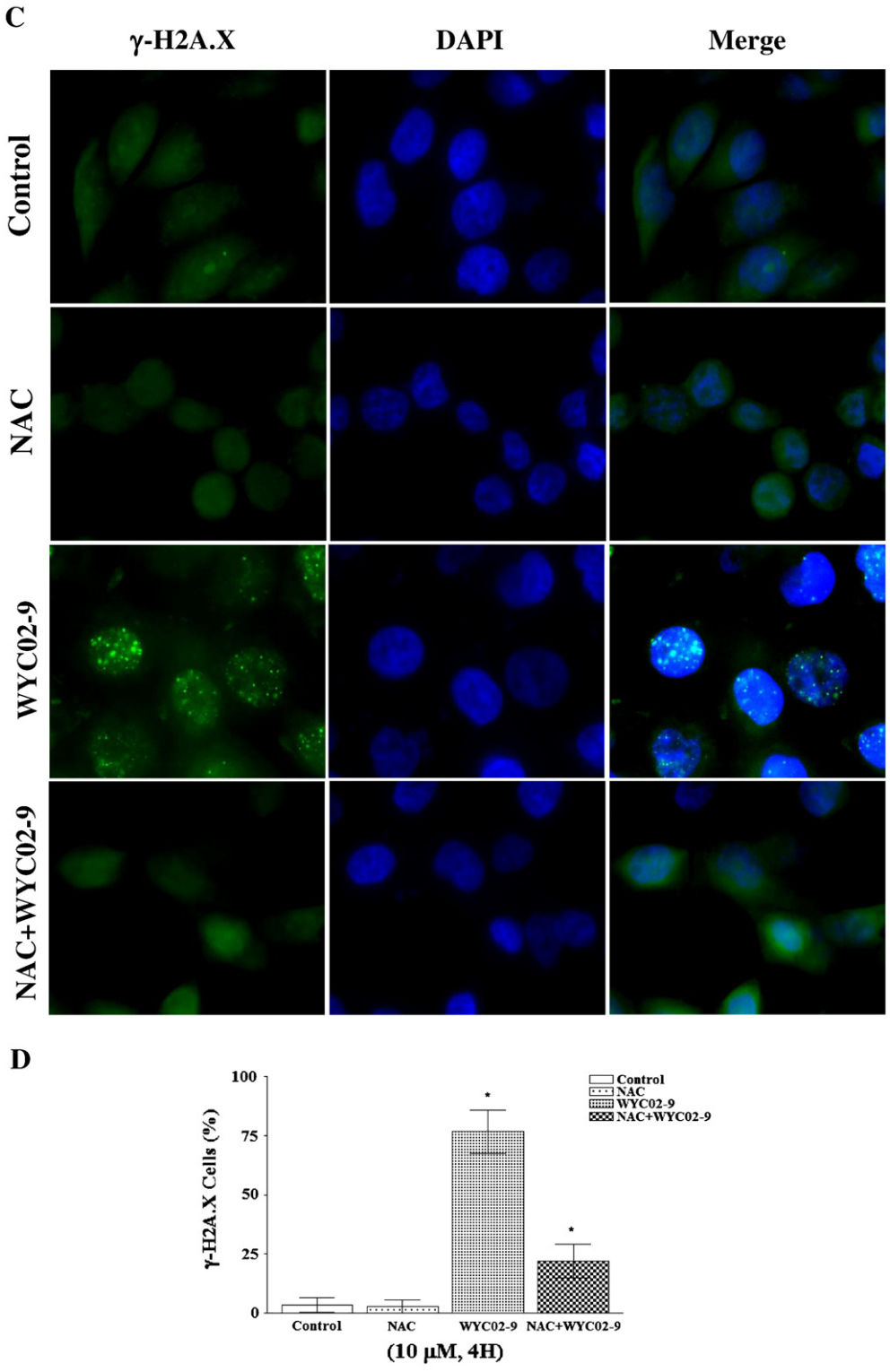

Fig. 3 (*continued*).

ethanol at −20 °C. Then, after two washes with 1× PBS, the cells were incubated with 1 μl of propidium iodide solution (50 μg/ml) in darkness for 30 min at room temperature. The relative DNA content of these cells was analyzed by FACScan cytometry (Becton–Dickinson) based on red fluorescence. Quantification of the fraction of each cell cycle stage was performed with ModFit LT for Mac 3.0 software (Becton–Dickinson).

Cell morphology analysis

DU145 cells grown on 6-cm dishes were treated with WYC02-9 at dosages of 0, 5, or 10 μM alone or combined with a given inhibitor for 24 h. The morphological changes were observed under an inverted microscope (Nikon TS100).

Annexin V/PI apoptosis assay

Annexin V/PI was used to detect early apoptotic cells during apoptotic progression. After treatment with WYC02-9 alone or combined with a given inhibitor for 24 h, the cells were trypsinized and washed twice with cold PBS and then adjusted to 5×10^5 cells/500 μl in binding buffer containing annexin V–FITC (1 μg/ml) and PI before analysis by flow cytometry (Becton–Dickinson). Detailed procedure was followed according to the manufacturer's instructions (Strong Biotech, Taipei, Taiwan).

Nude mice xenograft study

Human prostate cancer cells DU145 (3×10^6) were suspended in 0.1 ml PBS and injected subcutaneously into the right flank of 4-week-old male nude mice (BALB/cAnN-Foxn1nu/CrlNarl) purchased from the National Science Council Animal Center (Taipei, Taiwan). When tumors became visible (approximately 3×3 mm in size, roughly 7 days), the mice were randomly grouped and treated intraperitoneally with WYC02-9 or vehicle every other day for 8 weeks. The control group, low-dose group, and high-dose group were given individually PBS or 0.0608 or 0.608 μg/g body wt WYC02-9 in PBS (equal to one-tenth of the IC_{50} and the IC_{50} for DU145 cells, respectively). Tumor size was measured every other day using calipers and their volumes were calculated according to a standard formula: width$^2\times$length/2. Complete counts of the nude mouse blood were determined using SysmexXE-2100 (TOA Medical Electronics, Kobe, Japan), and the plasma BUN, Cr, AST, and ALT levels were determined by Beckman LX20 (Beckman–Coulter, Fullerton, CA, USA).

Immunohistochemistry analysis

The tumor tissue samples were fixed with 10% buffered formalin, dehydrated, embedded in paraffin, and sectioned to 3-μm thickness. In brief, tissue slides were deparaffinized in xylene and rehydrated in a gradient of ethanol. Subsequently, endogenous peroxidase activity was quenched with 3% hydrogen peroxide. To unmask antigen, the slides were submerged in 95 °C citrate buffer (10 mM, pH 6.0) or in EDTA buffer (1 mM, pH 8.0) for 15 min. The tissues were blocked for 15 min with a protein blocking, serum-free reagent (Dako Cytomation, Mississauga, ON, Canada) and incubated with various antibodies for 90 min at room temperature in a humid chamber. The optimal concentration for each primary antibody was determined by serial dilutions. Biotinylated secondary antibody (Dako Cytomation) was applied to the tissue sections and developed with streptavidin horseradish peroxidase (Dako Diagnostics Canada, Mississauga, ON, Canada). Hematoxylin was used as a counterstain. The results were captured by a Nikon TS100 microscope and then processed by Adobe PhotoImpact 12.

Statistics

Results are presented as means ± SD and comparisons were made using Student's *t* test. A probability of 0.05 or less was considered statistically significant.

Results

Effects of WYC02 and WYC02-9 on cell viability in DU145 PCA cells

To investigate the biological effects of the synthetic protoapigenone WYC02 and one of its derivatives, WYC02-9, DU145 cells were treated with various doses of WYC02 and WYC02-9 (0, 2.5, 5, 10 μM) for 24 h and the cell viability was assayed. Both WYC02 and WYC02-9 showed a dose-dependent suppression of cell viability (Fig. 1B). The IC_{50} values of WYC02 and WYC02-9 were 5.9 ± 0.6 and 2.0 ± 0.2 μM, respectively.

Effect of WYC02-9 on clonogenic formation in PCA DU145 cells

Additional experiments were done to determine the anti-cancer activity of WYC02-9, which showed a superior effect on the inhibition of cell survival compared to WYC02, by clonogenic assays. As shown in Fig. 1C, clonogenicity was reduced in a concentration-dependent manner after treatment with WYC02-9 in DU145 cells.

Effect of WYC02-9 on ROS generation in DU145 cells

Intracellular ROS levels were determined by flow cytometry using the H_2DCF-DA fluorescent probe. Cells treated with 10 μM WYC02-9 showed a time-dependent increase in ROS production (Figs. 2A and B). However, pretreatment of DU145 cells with the ROS scavenger NAC at 10 mM for 4 h blocked WYC02-9-induced ROS formation (Figs. 2C and D). These results revealed that ROS accumulation triggered by WYC02-9 was significantly suppressed by NAC pretreatment.

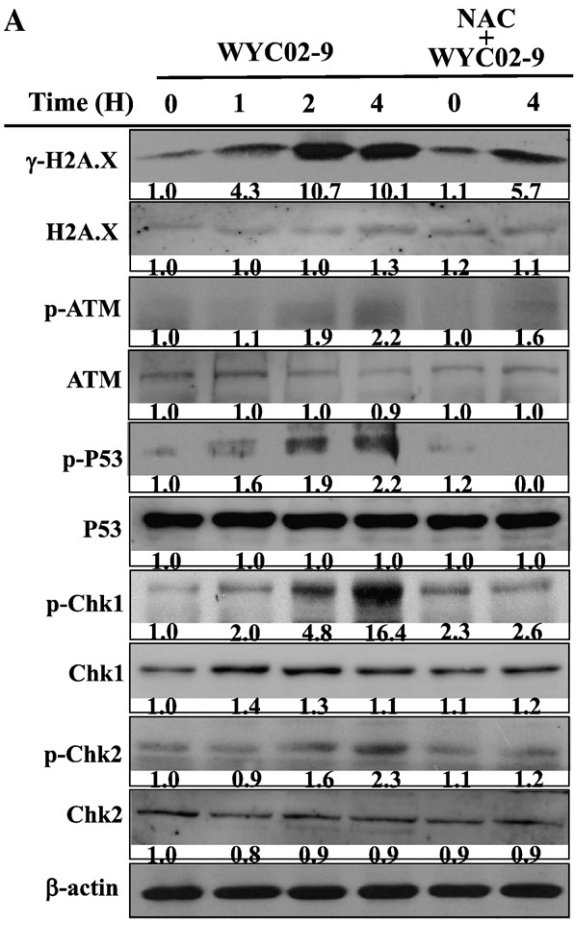

Fig. 4. Effect of WYC02-9 on induction of DNA-damage-sensing kinases in DU145 cells. (A) Cells were harvested and lysates were prepared and subjected to SDS–PAGE followed by immunoblotting for γ-H2A.X, H2A.X, p-ATM, ATM, p-p53, p53, p-Chk1, Chk1, p-Chk2, Chk2, and β-actin. β-Actin was used as the loading control. (B) Effect of WYC02-9-induced cell cycle arrest in DU145 cells. The cell cycle distribution revealed two major peaks at S and G2/M phases based on the DNA content. (C) Effect of NAC on cell cycle distribution in WYC02-9-treated DU145 cells. Data are presented as means ± SD of three independent experiments. *$P<0.05$ compared with untreated control. ATM, ataxia telangiectasia mutated; NAC, *N*-acetylcysteine.

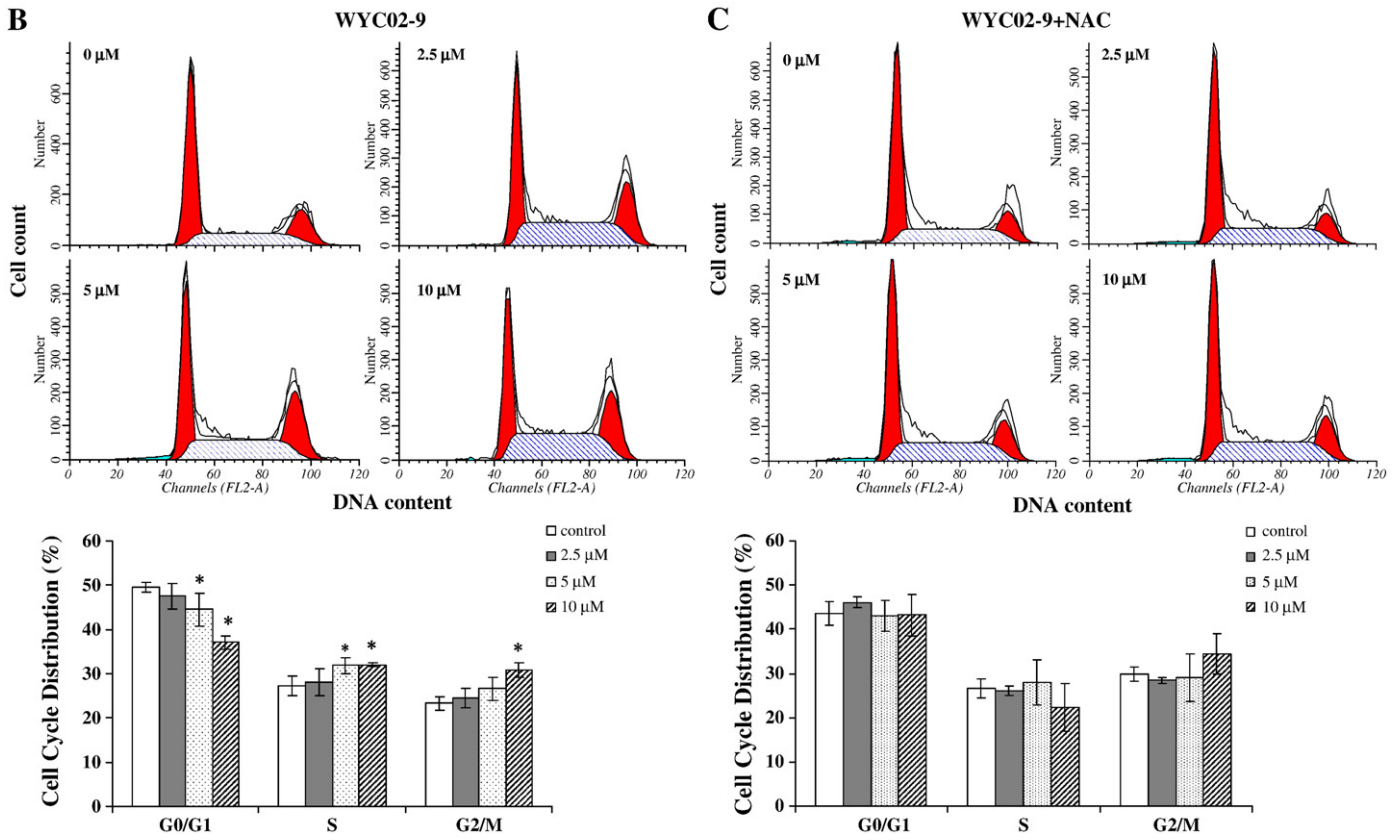

Fig. 4 (*continued*).

Effect of WYC02-9 on the induction of DNA double-strand breaks and γ-H2A.X focus formation in DU145 cells

Cells were pretreated with or without 10 mM NAC for 4 h, followed by treatment with 10 μM WYC02-9 for the indicated times. In the comet assay, DNA migration represents DSBs. Images of representative nuclei are shown in Fig. 3A. DSBs showed a time-dependent increase in the WYC02-9-treated group (Fig. 3B). NAC significantly protected cells from WYC02-9-induced DNA double-strand breaks (Figs. 3A and B).

Phosphorylation of H2A.X (known as γ-H2A.X), a histone H2A variant, is the most studied chromatin modification induced by DSBs. γ-H2A.X focus formation involves the spreading of γ-H2A.X from the DSBs into very large domains of surrounding chromatin [31]. As shown in Figs. 3C and D, immunofluorescent staining of γ-H2A.X foci was increased in WYC02-9-treated cells and NAC pretreatment effectively inhibited WYC02-9-induced γ-H2A.X focus formation.

Effects of WYC02-9 on the activation of DNA-damage-sensing kinases and cell cycle progression in DU145 cells

Expression of DNA-damage-related proteins, including γ-H2A.X, p-ATM, p-p53, p-Chk1, and p-Chk2, as well as their total levels, was analyzed by immunoblot. Treatment of DU145 cells with WYC02-9 resulted in up-regulation of γ-H2A.X, p-ATM, p-p53, p-Chk1, and p-Chk2. However, NAC pretreatment decreased WYC02-9-activated γ-H2A.X, p-ATM, p-p53, p-Chk1, and p-Chk2 expression. The total levels of H2A.X, ATM, Chk1, and Chk2 were only slightly changed (Fig. 4A).

As for the effect of WYC02-9 on cell cycle progression, DU145 cells were pretreated with or without 10 mM NAC for 4 h, followed by treatment with 0, 2.5, 5, or 10 μM WYC02-9 for 24 h. The results showed that treatment with WYC02-9 increased cells in both S and G2/M phases and decreased cells at G1 phase compared to untreated control cells (Fig. 4B). Pretreatment with NAC prevented the WYC02-9-increased cell cycle arrest in S and G2/M phases (Fig. 4C).

Effect of WYC02-9 on $\Delta\Psi_m$ and apoptotic cell death in DU145 cells

The integrity of the mitochondrial membranes in cells was examined by rhodamine 123 staining, and the decrease in rhodamine 123 fluorescence intensity reflected $\Delta\Psi_m$ decrease. Cells were pretreated with or without 10 mM NAC for 4 h, followed by treatment with 10 μM WYC02-9 for the indicated times. As shown in Figs. 5A and B, treatment with WYC02-9 resulted in a decrease in $\Delta\Psi_m$ and NAC pretreatment reversed the WYC02-9-induced decrease in $\Delta\Psi_m$.

Further cell morphology analysis, cell viability assay, and annexin V/PI apoptosis assay also showed that treatment with WYC02-9 resulted in a dose-dependent increase in apoptotic cell death and this effect was reduced by NAC pretreatment (Figs. 5C–E). WYC02-9 induced caspase-9 and caspase-3 activation, as well as PARP cleavage in a dose-dependent manner. However, NAC pretreatment decreased WYC02-9-activated caspase-9 and caspase-3 as well as PARP cleavage expression (Fig. 5F).

Effect of WYC02-9 on the growth of DU145 tumor xenografts in nude mice

Nude mice bearing DU145 xenografts were treated with WYC02-9 every other day for 8 weeks. As shown in Fig. 6A, treatment with high-dose WYC02-9 resulted in a significant decrease in

tumor size (190.7 ± 40.0 mm^3) compared to low-dose WYC02-9 (346.2 ± 107.2 mm^3) and control (502.0 ± 76.8 mm^3) groups. DU145 tumor xenografts from vehicle-treated and WYC02-9-treated mice were also analyzed for γ-H2A.X, caspase-9, caspase-3, and PARP. The results showed that γ-H2A.X, caspase-9, and caspase-3 activation, as well as PARP cleavage, was increased in

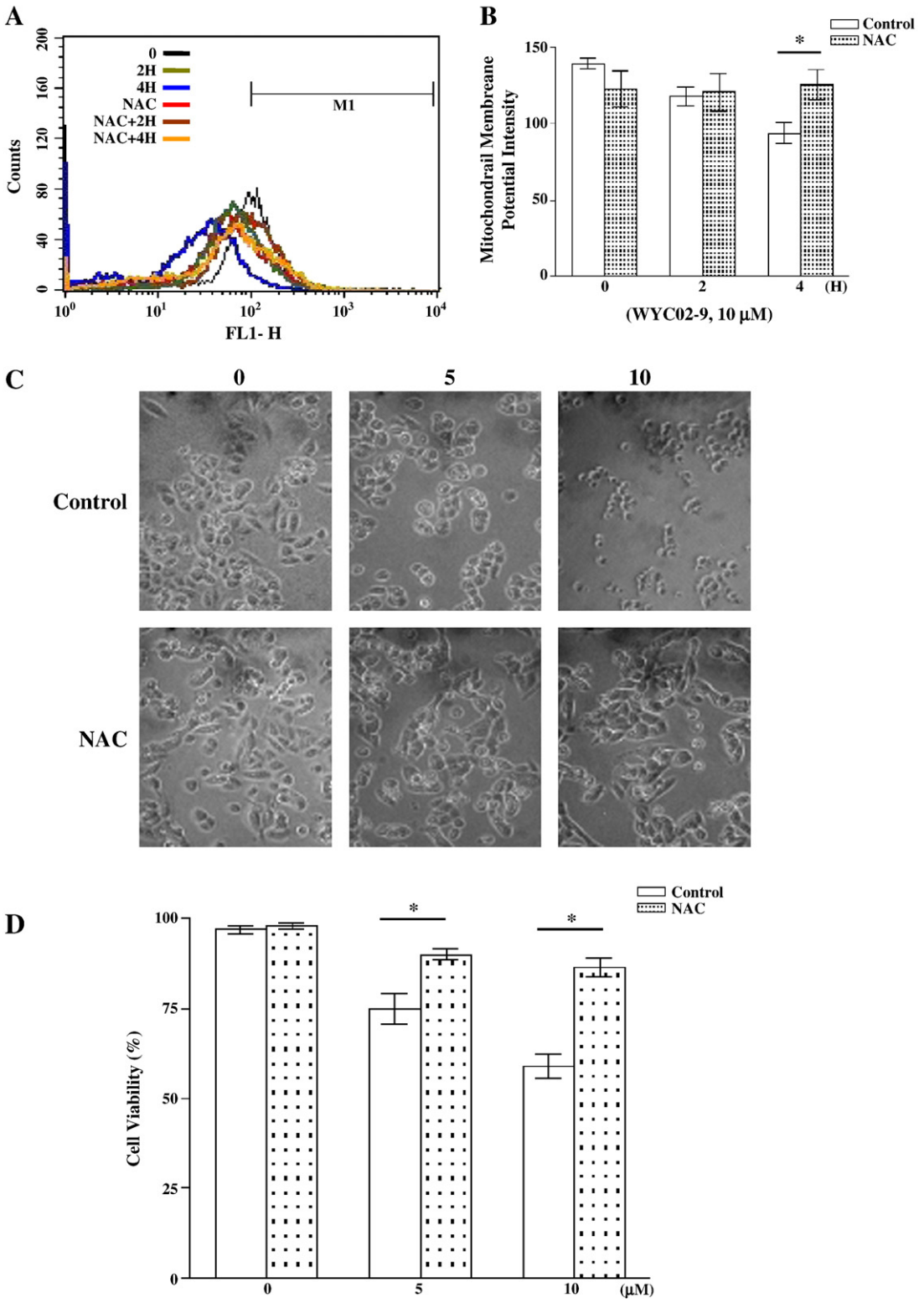

Fig. 5. Effect of WYC02-9 on induction of $\Delta\Psi_m$ decrease and apoptosis in DU145 cells. (A) Cells were incubated with 10 μM rhodamine 123 for 30 min, followed by flow cytometry analysis. (B) Quantified data from (A) are presented as means ± SD of three independent experiments. (C) Microphotographs of the inhibitory effect on cell growth. The photographs were taken directly from culture plates with a phase microscope (original magnification × 100). (D) Percentage of cell viability determined by cell viability assay. (E) Percentage of apoptosis by annexin V/PI staining followed by FACS flow cytometry analysis. (F) Cells were harvested and lysates were prepared and subjected to SDS–PAGE followed by immunoblotting for caspase-9, caspase-3, PARP, and β-actin. β-Actin was used as the loading control. Data are presented as means ± SD of three independent experiments. *$P<0.05$ compared with the respective controls treated with WYC02-9 alone. $\Delta\Psi_m$, mitochondrial transmembrane potential; NAC, *N*-acetylcysteine; PARP, poly(ADP-ribose) polymerase.

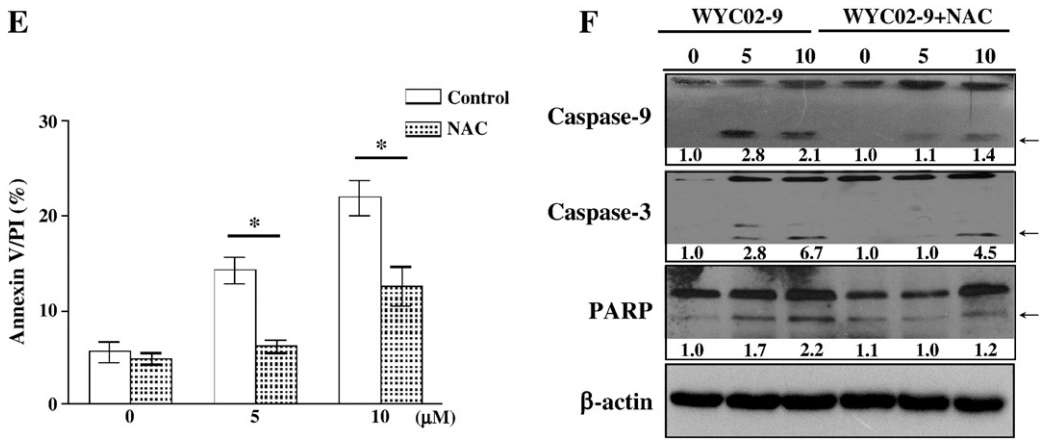

Fig. 5 (*continued*).

both high-dose and low-dose WYC02-9 groups (Fig. 6B). Immunohistochemistry staining of excised tumor sections also revealed a higher expression of both γ-H2A.X and cleaved PARP in WYC02-9-treated tumors (Fig. 6C).

Regarding the side effects of WYC02-9 on nude mice, no significant difference was found in body weight among control and WYC02-9-treated groups (Fig. 6D). Blood chemistry values were within normal limits, except for an inhibitory effect on white blood cell counts with

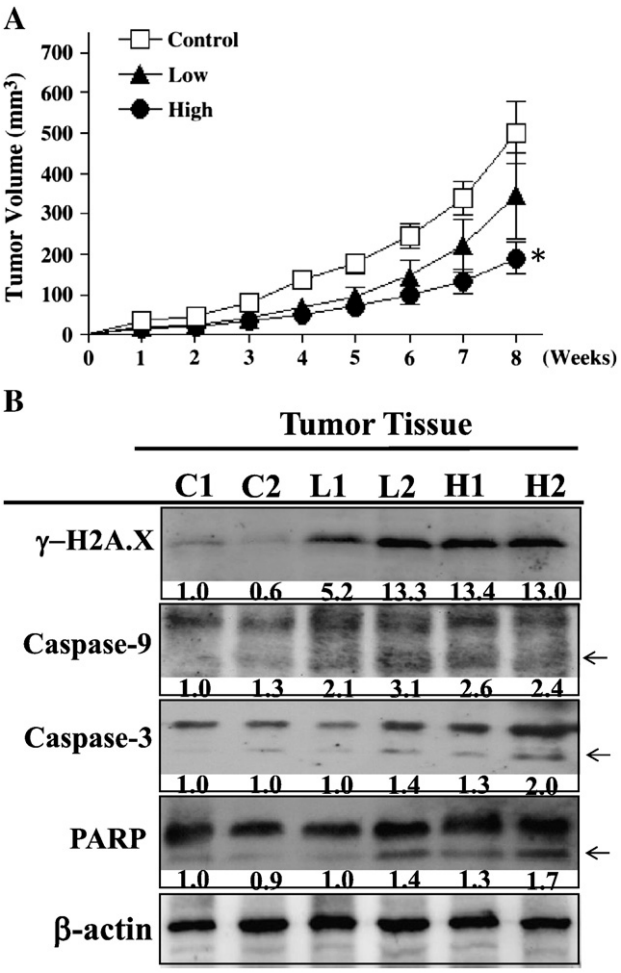

Fig. 6. Effect of WYC02-9 on DU145 tumor growth in nude mouse xenograft model. (A) During the 8 weeks treatment with WYC02-9 or vehicle, tumor volumes were measured using external calipers (mm^3) weekly for each group, and the data are presented as means ± SEM. (B) Tumor xenografts from vehicle-treated and WYC02-9-treated mice were analyzed for γ-H2A.X, caspase-9, caspase-3, PARP, and β-actin by immunoblotting. β-Actin was used as the loading control. (C) Representative tumor sections of vehicle-treated mice and WYC02-9-treated mice were stained for γ-H2A.X and cleaved PARP. (D) The mean body weight in control and WYC02-9-treated groups. Data are presented as means ± SD. C1 and C2, control group; L1 and L2, low-dose group; H1 and H2, high-dose group. *$P<0.05$ compared with untreated control and low-dose WYC02-9 groups. PARP, poly(ADP-ribose) polymerase.

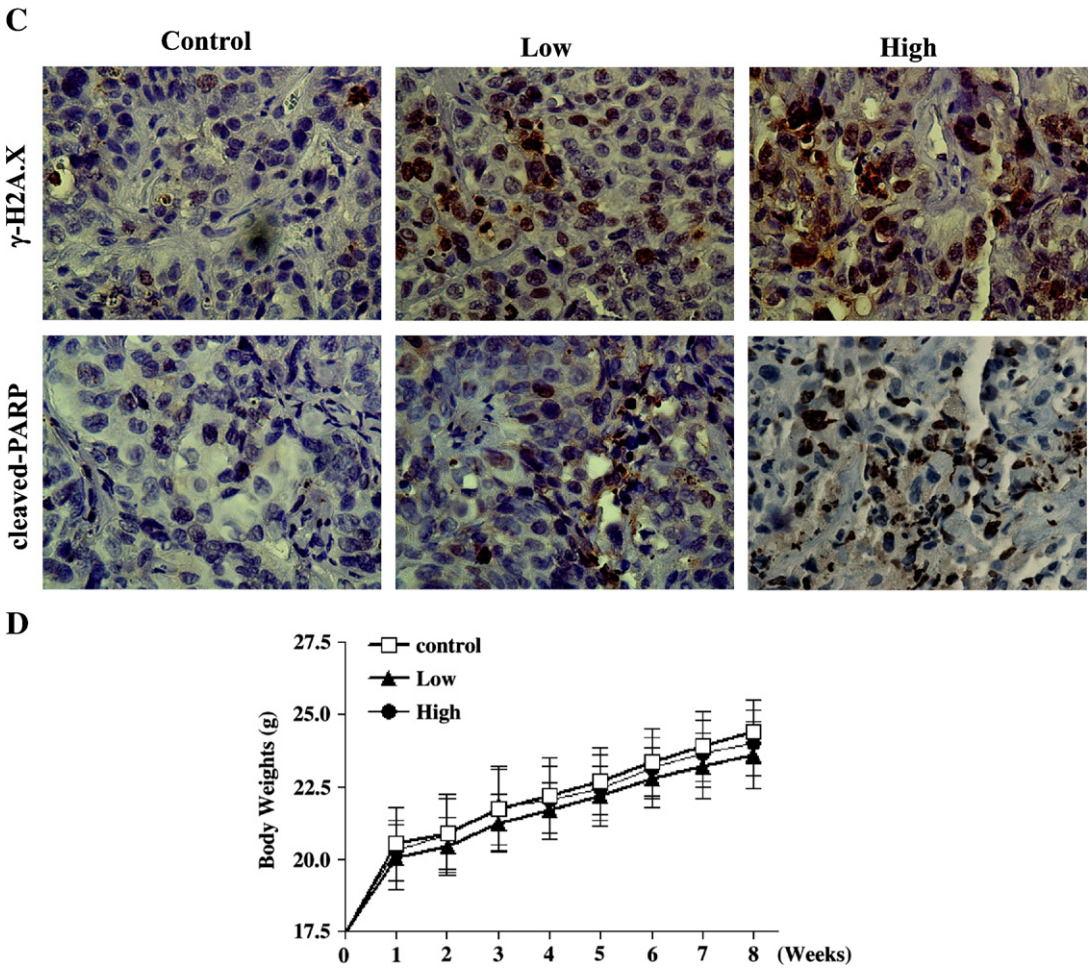

Fig. 6 (*continued*).

the high-dose WYC02-9 compared to both low-dose WYC02-9 and control groups (Table 1).

Discussion

The synthetic protoapigenone analogue WYC02-9 contains higher cytotoxic activity than synthetic protoapigenone (WYC02) in cell lines derived from liver, breast, and lung cancers [3]. In this study, we found that WYC02-9 inhibited cell growth of PCA DU145 cells more significantly than WYC02 (Fig. 1B). Moreover, treatment of DU145 cells with WYC02-9 induced an approximately twofold increase in ROS generation and this effect was accompanied by an induction of DNA damage, cell cycle arrest, and mitochondrial-dependent cell apoptosis, which were blocked by NAC, a ROS scavenger [32]. These findings therefore suggest that WYC02-9-induced DNA damage and apoptosis in DU145 cells are mediated at least partly via ROS generation.

WYC02-9 is a novel compound synthesized by structural modification of WYC02 with the addition of a conjugated aromatic ring on the A-ring (Fig. 1A). In this study, we found that WYC02-9 efficiently

Table 1
The complete blood count and biochemical profile for the nude mice after treatment with WYC02-9 every other day for 8 weeks.

	Control (N = 10)	Low dose (N = 10)	High dose (N = 10)
WBC (10×3/μl)	3.1 ± 0.8	2.9 ± 0.8	2.0 ± 0.7
RBC (10×6/μl)	8.6 ± 0.4	8.6 ± 0.4	8.6 ± 0.7
HGB (g/dl)	12.8 ± 0.6	13.0 ± 0.8	13.2 ± 1.2
HCT (%)	39.8 ± 2.2	40.4 ± 2.8	40.6 ± 4.1
MCV (fl)	46.6 ± 1.5	46.8 ± 1.7	47.0 ± 1.5
MCH (pg)	15.0 ± 0.4	15.0 ± 0.4	15.3 ± 0.5
MCHC (%)	32.1 ± 0.7	32.1 ± 0.5	32.6 ± 1.5
PLT (10×3/μl)	675.7 ± 94.6	627.5 ± 134.5	581.9 ± 117.7
AST(GOT) (U/L)	81.6 ± 81.7	65.3 ± 37.8	79.1 ± 46.3
ALT(GPT) (U/L)	26.0 ± 6.0	25.6 ± 7.3	31.0 ± 10.3
BUN (mg/dl)	21.1 ± 2.6	21.7 ± 2.4	24.6 ± 4.3
Creatinine (mg/dl)	0.4 ± 0.0	0.4 ± 0.1	0.3 ± 0.1

The data are presented as means ± SD.
$P<0.05$ as compared with the control group.

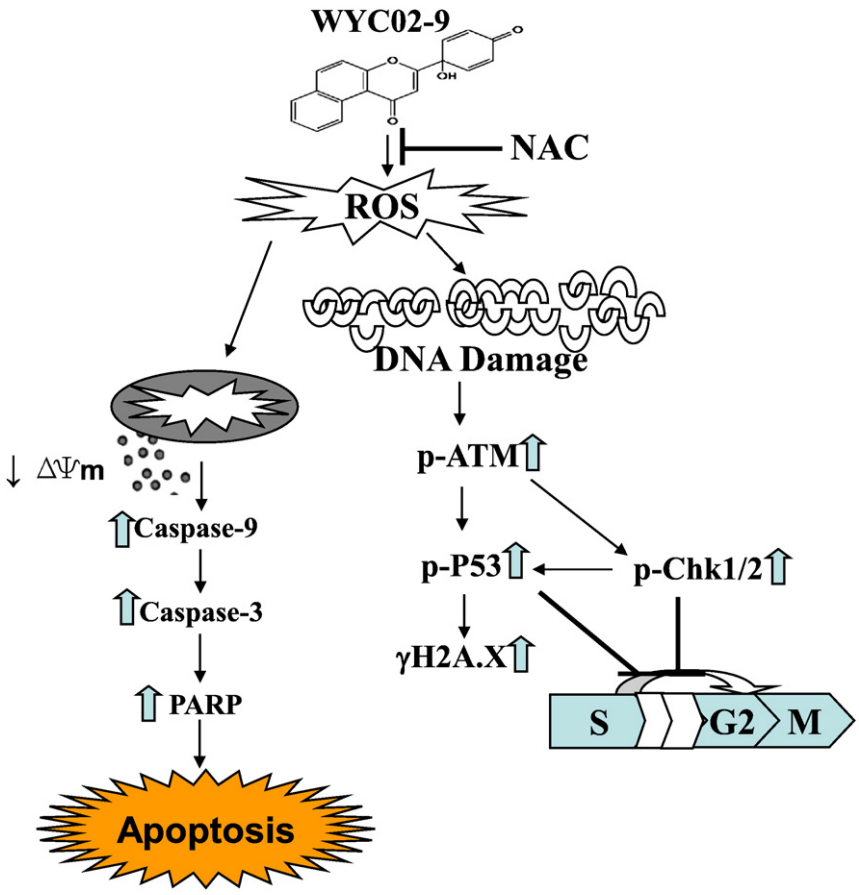

Fig. 7. A schematic diagram showing the proposed model for the mechanism of action of WYC02-9 on various biochemical processes in DU145 cells.

inhibited cell growth of human PCA cell lines, including DU145, PC-3, and LNCaP, with the most significant cytotoxicity on DU145 cells (data not shown). This cytotoxicity was further confirmed by clonogenic formation assay, showing an irreversible loss of long-term clonogenic growth ability in WYC02-9-treated DU145 cells (Fig. 1C).

ROS generation in several anti-cancer therapies has been reported to contribute to their anti-cancer activities. Manipulation of ROS generation in cancer cells has also been reported to be a potential therapeutic strategy to enhance the cytotoxicity of drugs [12,26,33–35]. In this study, we found that treatment with WYC02-9 greatly increased ROS production and cytotoxicity in DU145 cells (Figs. 2A–D). The increased oxidative stress has been shown to cause DNA damage, followed by cell cycle arrest in cancer cells [6,12,13,26]. In this study, we assessed DSBs by two approaches, comet assay and γ-H2A.X foci formation assay [17,36,37]. Both assays provided clear evidence of DSB induction by WYC02-9 treatment; however, quenching ROS with NAC diminished WYC02-9-mediated DSB formation in DU145 cells (Figs. 3A–D). In addition, NAC has been reported to increase intracellular levels of glutathione (γ-glutamylcysteinyl glycine, or GSH) [32]. GSH is thought to be an important factor in cellular function and defense against oxidative stress. Both NAC and GSH are capable of neutralizing ROS and conjugating with electrophiles [32,38]. Thus, apart from scavenging ROS, NAC is also postulated to protect cells by increasing intracellular GSH levels. Based on these studies, glutathione may have a role in WYC02-9-mediated ROS production. Nonetheless, this needs to be further clarified.

Induction of DSBs triggers H2A.X phosphorylation through activation of the ATM–p53-mediated cell cycle control pathways [39–41]. The cell cycle checkpoint kinases Chk1 and Chk2, downstream of ATM, also activate p53 in response to DNA damage [40,42]. In this study, the activation of the ATM–p53 pathway and checkpoint proteins Chk1/Chk2 further supported the existence of DSBs after WYC02-9 treatment in DU145 cells (Fig. 4A). However, pretreatment with NAC attenuated all of the above effects, suggesting that WYC02-9-induced DNA damage and cell cycle arrest in S and G2/M phases in DU145 cells were mediated via ROS generation (Figs. 4A–C).

Mitochondria, being the main site of ROS generation in the cell, are also their primary target. ROS can cause a decrease in $\Delta\Psi_m$, leading to caspase activation and cell apoptosis [43,44]. In this study, we found that WYC02-9 induced a decrease in $\Delta\Psi_m$, activation of caspase-9 and −3, and cleavage of PARP, as well as cell apoptosis in DU145 cells, and these effects were significantly blocked by pretreatment with NAC (Figs. 5A, E, and F). These results suggested that WYC02-9 induced mitochondrial-dependent cell apoptosis by generating ROS in DU145 cells. Furthermore, in the DU145 mouse xenograft study, administration of WYC02-9 resulted in a reduction in tumor volume (Fig. 6A) and an increase γ-H2A.X, caspase-9 and caspase-3 activity, and PARP cleavage (Figs. 6B and C). These findings are consistent with in vitro studies, thus confirming the mechanisms of the anti-cancer effects of WYC02-9 on DU145 cells.

In conclusion, WYC02-9 induced ROS formation and led to DNA damage as well as increasing the number of cells in S and G2/M phases through the ATM–p53–H2A.X dependent pathway. On the other hand, the accumulation of ROS by WYC02-9 triggered mitochondrial-dependent cell apoptosis through activation of caspase-9, caspase-3, and PARP (Fig. 7). Administration of WYC02-9 also inhibited the growth of DU145 tumors in the xenograft model. Thus, both in vitro and in vivo studies suggest that WYC02-9 has the potential to be developed into an effective anti-cancer agent in the clinical setting.

Acknowledgments

We thank Professors Lih-Wen Fang (I-Shou University, Taiwan), Mei-Chin Lu (National Dong Hwa University, Taiwan), and Sushil Mandal (E-Da Hospital/I-Shou University, Taiwan), for critically reading the manuscript. This work was supported by National Health Research Institutes Grant NHRI-EX99-9829BI, National Science Council Grant NSC 97-2314-B-214, E-DA Hospital Grants EDAH-98004 and EDAHP99022, and Department of Health DOH99-TD-C-111-002, Taiwan, Republic of China.

References

[1] Havsteen, B. H. The biochemistry and medical significance of the flavonoids. *Pharmacol. Ther.* **96:**67–202; 2002.
[2] Middleton Jr., E.; Kandaswami, C.; Theoharides, T. C. The effects of plant flavonoids on mammalian cells: implications for inflammation, heart disease, and cancer. *Pharmacol. Rev.* **52:**673–751; 2000.
[3] Lin, A. S.; Nakagawa-Goto, K.; Chang, F. R.; Yu, D.; Morris-Natschke, S. L.; Wu, C. C.; Chen, S. L.; Wu, Y. C.; Lee, K. H. First total synthesis of protoapigenone and its analogues as potent cytotoxic agents. *J. Med. Chem.* **50:**3921–3927; 2007.
[4] Chang, H. L.; Wu, Y. C.; Su, J. H.; Yeh, Y. T.; Yuan, S. S. Protoapigenone, a novel flavonoid, induces apoptosis in human prostate cancer cells through activation of p38 mitogen-activated protein kinase and c-Jun NH_2-terminal kinase 1/2. *J. Pharmacol. Exp. Ther.* **325:**841–849; 2008.
[5] Chang, H. L.; Su, J. H.; Yeh, Y. T.; Lee, Y. C.; Chen, H. M.; Wu, Y. C.; Yuan, S. S. Protoapigenone, a novel flavonoid, inhibits ovarian cancer cell growth in vitro and in vivo. *Cancer Lett.* **267:**85–95; 2008.
[6] Passos, J. F.; Saretzki, G.; von Zglinicki, T. DNA damage in telomeres and mitochondria during cellular senescence: is there a connection? *Nucleic Acids Res.* **35:**7505–7513; 2007.
[7] Powis, G. Free radical formation by antitumor quinones. *Free Radic. Biol. Med.* **6:** 63–101; 1989.
[8] Kotamraju, S.; Kalivendi, S. V.; Konorev, E.; Chitambar, C. R.; Joseph, J.; Kalyanaraman, B. Oxidant-induced iron signaling in doxorubicin-mediated apoptosis. *Meth. Enzymol.* **378:**362–382; 2004.
[9] Wang, H.; Mao, Y.; Chen, A. Y.; Zhou, N.; LaVoie, E. J.; Liu, L. F. Stimulation of topoisomerase II-mediated DNA damage via a mechanism involving protein thiolation. *Biochemistry* **40:**3316–3323; 2001.
[10] Ames, B. N. Dietary carcinogens and anticarcinogens: oxygen radicals and degenerative diseases. *Science* **221:**1256–1264; 1983.
[11] Lu, H. R.; Meng, L. H.; Huang, M.; Zhu, H.; Miao, Z. H.; Ding, J. DNA damage, c-myc suppression and apoptosis induced by the novel topoisomerase II inhibitor, salvicine, in human breast cancer MCF-7 cells. *Cancer Chemother. Pharmacol.* **55:**286–294; 2005.
[12] Wang, J.; Yi, J. Cancer cell killing via ROS: to increase or decrease, that is the question. *Cancer Biol. Ther.* **7:**1875–1884; 2008.
[13] Trachootham, D.; Zhou, Y.; Zhang, H.; Demizu, Y.; Chen, Z.; Pelicano, H.; Chiao, P. J.; Achanta, G.; Arlinghaus, R. B.; Liu, J.; Huang, P. Selective killing of oncogenically transformed cells through a ROS-mediated mechanism by beta-phenylethyl isothiocyanate. *Cancer Cell* **10:**241–252; 2006.
[14] Chen, H. M.; Wu, Y. C.; Chia, Y. C.; Chang, F. R.; Hsu, H. K.; Hsieh, Y. C.; Chen, C. C.; Yuan, S. S. Gallic acid, a major component of Toona sinensis leaf extracts, contains a ROS-mediated anti-cancer activity in human prostate cancer cells. *Cancer Lett.* **286:**161–171; 2009.
[15] Wang, S.; Konorev, E. A.; Kotamraju, S.; Joseph, J.; Kalivendi, S.; Kalyanaraman, B. Doxorubicin induces apoptosis in normal and tumor cells via distinctly different mechanisms: intermediacy of H_2O_2- and p53-dependent pathways. *J. Biol. Chem.* **279:**25535–25543; 2004.
[16] Brem, R.; Li, F.; Montaner, B.; Reelfs, O.; Karran, P. DNA breakage and cell cycle checkpoint abrogation induced by a therapeutic thiopurine and UVA radiation. *Oncogene* **29:**3953–3963; 2010.
[17] Mroz, R. M.; Schins, R. P.; Li, H.; Jimenez, L. A.; Drost, E. M.; Holownia, A.; MacNee, W.; Donaldson, K. Nanoparticle-driven DNA damage mimics irradiation-related carcinogenesis pathways. *Eur. Respir. J.* **31:**241–251; 2008.
[18] Yang, J. S.; Chen, G. W.; Hsia, T. C.; Ho, H. C.; Ho, C. C.; Lin, M. W.; Lin, S. S.; Yeh, R. D.; Ip, S. W.; Lu, H. F.; Chung, J. G. Diallyl disulfide induces apoptosis in human colon cancer cell line (COLO 205) through the induction of reactive oxygen species, endoplasmic reticulum stress, caspases cascade and mitochondrial-dependent pathways. *Food Chem. Toxicol.* **47:**171–179; 2009.
[19] Ko, C. H.; Shen, S. C.; Hsu, C. S.; Chen, Y. C. Mitochondrial-dependent, reactive oxygen species-independent apoptosis by myricetin: roles of protein kinase C, cytochrome c, and caspase cascade. *Biochem. Pharmacol.* **69:**913–927; 2005.
[20] Lu, H. F.; Hsueh, S. C.; Ho, Y. T.; Kao, M. C.; Yang, J. S.; Chiu, T. H.; Huamg, S. Y.; Lin, C. C.; Chung, J. G. ROS mediates baicalin-induced apoptosis in human promyelocytic leukemia HL-60 cells through the expression of the Gadd153 and mitochondrial-dependent pathway. *Anticancer Res.* **27:**117–125; 2007.
[21] Jemal, A.; Murray, T.; Ward, E.; Samuels, A.; Tiwari, R. C.; Ghafoor, A.; Feuer, E. J.; Thun, M. J. Cancer statistics, 2005. *CA Cancer J. Clin.* **55:**10–30; 2005.
[22] Jemal, A.; Siegel, R.; Ward, E.; Hao, Y.; Xu, J.; Murray, T.; Thun, M. J. Cancer statistics, 2008. *CA Cancer J. Clin.* **58:**71–96; 2008.
[23] Pu, Y. S.; Chiang, H. S.; Lin, C. C.; Huang, C. Y.; Huang, K. H.; Chen, J. Changing trends of prostate cancer in Asia. *Aging Male* **7:**120–132; 2004.
[24] Klein, E. A. Chemoprevention of prostate cancer. *Annu. Rev. Med.* **57:**49–63; 2006.
[25] Sharifi, N.; Gulley, J. L.; Dahut, W. L. Androgen deprivation therapy for prostate cancer. *JAMA* **294:**238–244; 2005.
[26] Stadtman, E. R.; Berlett, B. S. Reactive oxygen-mediated protein oxidation in aging and disease. *Drug Metab. Rev.* **30:**225–243; 1998.
[27] Stephenson, A. J.; Abouassaly, R.; Klein, E. A. Chemoprevention of prostate cancer. *Urol. Clin. North Am.* **37:**11–21; 2010.
[28] Krishnaswamy, R.; Devaraj, S. N.; Padma, V. V. Lutein protects HT-29 cells against deoxynivalenol-induced oxidative stress and apoptosis: prevention of NF-κB nuclear localization and down regulation of NF-κB and cyclo-oxygenase-2 expression. *Free Radic. Biol. Med.* **49:**50–60; 2010.
[29] Singh, R. P.; Dhanalakshmi, S.; Agarwal, R. Phytochemicals as cell cycle modulators—a less toxic approach in halting human cancers. *Cell Cycle* **1:** 156–161; 2002.
[30] Chang, H. L.; Hsu, H. K.; Su, J. H.; Wang, P. H.; Chung, Y. F.; Chia, Y. C.; Tsai, L. Y.; Wu, Y. C.; Yuan, S. S. The fractionated Toona sinensis leaf extract induces apoptosis of human ovarian cancer cells and inhibits tumor growth in a murine xenograft model. *Gynecol. Oncol.* **102:**309–314; 2006.
[31] Rogakou, E. P.; Pilch, D. R.; Orr, A. H.; Ivanova, V. S.; Bonner, W. M. DNA double-stranded breaks induce histone H2AX phosphorylation on serine 139. *J. Biol. Chem.* **273:**5858–5868; 1998.
[32] Mi, L.; Sirajuddin, P.; Gan, N.; Wang, X. A cautionary note on using *N*-acetylcysteine as an antagonist to assess isothiocyanate-induced reactive oxygen species-mediated apoptosis. *Anal. Biochem.* **405:**269–271; 2010.
[33] Fruehauf, J. P.; Meyskens Jr., F. L. Reactive oxygen species: a breath of life or death? *Clin. Cancer Res.* **13:**789–794; 2007.
[34] D'Autreaux, B.; Toledano, M. B. ROS as signalling molecules: mechanisms that generate specificity in ROS homeostasis. *Nat. Rev. Mol. Cell Biol.* **8:**813–824; 2007.
[35] Renschler, M. F. The emerging role of reactive oxygen species in cancer therapy. *Eur. J. Cancer* **40:**1934–1940; 2004.
[36] Powell, S. N.; Bindra, R. S. Targeting the DNA damage response for cancer therapy. *DNA Repair (Amsterdam)* **8:**1153–1165; 2009.
[37] Agarwal, C.; Tyagi, A.; Agarwal, R. Gallic acid causes inactivating phosphorylation of cdc25A/cdc25C–cdc2 via ATM–Chk2 activation, leading to cell cycle arrest, and induces apoptosis in human prostate carcinoma DU145 cells. *Mol. Cancer Ther.* **5:** 3294–3302; 2006.
[38] Sato, N.; Ueno, T.; Kubo, K.; Suzuki, T.; Tsukimura, N.; Att, W.; Yamada, M.; Hori, N.; Maeda, H.; Ogawa, T. *N*-acetyl cysteine (NAC) inhibits proliferation, collagen gene transcription, and redox stress in rat palatal mucosal cells. *Dent. Mater.* **25:** 1532–1540; 2009.
[39] Kastan, M. B.; Lim, D. S. The many substrates and functions of ATM. *Nat. Rev. Mol. Cell Biol.* **1:**179–186; 2000.
[40] Bakkenist, C. J.; Kastan, M. B. DNA damage activates ATM through intermolecular autophosphorylation and dimer dissociation. *Nature* **421:**499–506; 2003.
[41] Ismail, I. H.; Nystrom, S.; Nygren, J.; Hammarsten, O. Activation of ataxia telangiectasia mutated by DNA strand break-inducing agents correlates closely with the number of DNA double strand breaks. *J. Biol. Chem.* **280:**4649–4655; 2005.
[42] Bakkenist, C. J.; Kastan, M. B. Initiating cellular stress responses. *Cell* **118:**9–17; 2004.
[43] Koka, P. S.; Mondal, D.; Schultz, M.; Abdel-Mageed, A. B.; Agrawal, K. C. Studies on molecular mechanisms of growth inhibitory effects of thymoquinone against prostate cancer cells: role of reactive oxygen species. *Exp. Biol. Med. (Maywood)* **235:**751–760; 2010.
[44] Green, D. R.; Reed, J. C. Mitochondria and apoptosis. *Science* **281:**1309–1312; 1998.